Engineering Science and Technology, an International Journal 19 (2016) 1108–1116

HOSTED BY

Contents lists available at ScienceDirect

Engineering Science and Technology, an International Journal

journal homepage: http://www.elsevier.com/locate/jestch

Full Length Article

Estimation of MHD boundary layer slip flow over a permeable stretching cylinder in the presence of chemical reaction through numerical and artificial neural network modeling

P. Bala Anki Reddy *, Raja Das

Department of Mathematics, SAS, VIT University, Vellore, Tamil Nadu 632014, India

ARTICLE INFO

Article history:
Received 16 July 2015
Received in revised form
23 November 2015
Accepted 9 December 2015
Available online 28 February 2016

Keywords:
Magnetohydrodynamics
Stretched cylinder
Artificial neural network
Back Propagation and chemical reaction

ABSTRACT

In this paper, the prediction of the magnetohydrodynamic boundary layer slip flow over a permeable stretched cylinder with chemical reaction is investigated by using some mathematical techniques, namely Runge–Kutta fourth order method along with shooting technique and artificial neural network (ANN). A numerical method is implemented to approximate the flow of heat and mass transfer characteristics as a function of some input parameters, explicitly the curvature parameter, magnetic parameter, permeability parameter, velocity slip, Grashof number, solutal Grashof number, Prandtl number, temperature exponent, Schmidt number, concentration exponent and chemical reaction parameter. The non-linear partial differential equations of the governing flow are converted into a system of highly non-linear ordinary differential equations by using the suitable similarity transformations, which are then solved numerically by a Runge–Kutta fourth order along with shooting technique and then ANN is applied to them. The Back Propagation Neural Network is applied for forecasting the desired outputs. The reported numerical values and the ANN values are in good agreement than those published works on various special cases. According to the findings of this study, the ANN approach is reliable, effective and easily applicable for simulating heat and mass transfer flow over a stretched cylinder.

1. Introduction

The study of boundary layer flow of heat and mass transfer of stretching flat plates or cylinders has attracted the interest of many researchers in view of its extensive applications in many industrial manufacturing processes that include both metal and polymer sheets. Some examples are in the extraction of polymer and rubber sheets, wire drawing, hot rolling, spinning of fibers, metal spinning, paper production, glass blowing, crystal growing, nuclear reactors, cooling of metallic sheets or electronic chips, manufacture of foods, etc. Crane [1] was the first among the others to consider an incompressible fluid flow due to a linearly stretching sheet. Enormous research works (Ali [2], Bachok et al. [3], Bhattacharya et al. [4], Chamka [5], Chethan et al. [6], Cortell [7], Das [8], Farahi Sahari and Hossein Nezhad [9], Grubka and Bobba [10], Hayat et al. [11], Hayat et al. [12], Ibrahim and Shanker [13], Pal and Chatterjee [14], Srinivas et al. [15], Srinivas et al. [16], Gupta and Gupta [17], Siddheshwar and Mahabaleshwar [18], Colonna and Capitelli [19], and Armenise et al. [20]) have been done on the boundary layer flow of heat and mass transfer over a stretching surface under different physical situations. In view of these applications, many researchers explored the boundary layer flow over a stretching surface under different physical situations. Laminar boundary layer along horizontal and vertical moving cylinders with constant velocity was discussed by Lin and Shih [21,22]. Wang [23] analyzed the viscous fluid flow outside a stretching cylinder obtained with an exact similarity solution. Heat and mass transfer from a permeable cylinder embedded in a porous medium with a magnetic field was studied by Chamka and Quadri [24]. Ishak et al. [25] explored the numerical solution of magnetohydrodynamic flow and heat transfer outside a stretching cylinder. The numerical solutions of the axisymmetric laminar boundary layer flow and heat transfer flow over a stretching cylinder were investigated by Ishak and Nazar [26] and Bachok and Ishak [27]. Hussam et al. [28] analyzed the heat transfer in MHD flow over a circular cylinder in duct with a Hartmann number. The axisymmetric laminar boundary layer mixed convection flow of a viscous incompressible fluid and heat transfer toward a stretching cylinder embedded in porous medium was studied by Mukhopadhyay [29]. Recently, Mukhopadhyay [30] explored the axisymmetric laminar boundary layer flow of a viscous

* Corresponding author. Tel: +91-8500132515.
E-mail address: pbarmaths@gmail.com (P.B.A. Reddy).
Peer review under responsibility of Karabuk University.

http://dx.doi.org/10.1016/j.jestch.2015.12.013

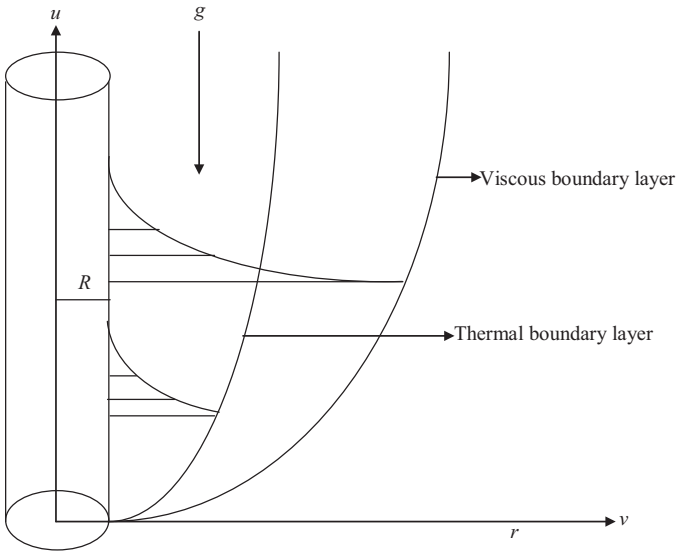

Fig. 1. Geometry of the problem.

incompressible fluid and heat transfer toward a stretching cylinder under the influence of a uniform magnetic field. Very recently, the influences of the temperature-dependent fluid properties and the transverse curvature on the axisymmetric flow and heat transfer at a horizontal permeable stretching cylinder were investigated by Vajravelu et al. [31].

To the best of the authors' knowledge, no investigation has been made yet to analyze the magnetohydrodynamic boundary layer slip flow over a permeable stretched cylinder with chemical reaction through ANN model. The literature review reveals that the ANN models have been quite promising in offering solutions to nonlinear problems. The ANN method has not been used for heat and mass transfer analysis of MHD boundary layer flow over a stretching cylinder. Therefore, the present study focuses on the applicability of the ANN method for the boundary layer flow over a stretching cylinder in the presence of chemical reaction. In this study, the influences of pertinent parameters on the flow and heat and mass transfer characteristics are analyzed, and the numerical results are presented in comparison with the results of ANN method.

This paper has been arranged as follows: Section 2 deals with the mathematical formulation of the problem. Numerical modeling and algorithm are presented in Section 3. Section 4 contains the importance and the discussion of ANN method and the Back Propagation algorithm. The concluding remarks are presented in Section 5.

2. Mathematical analysis

Let us consider the steady axisymmetric mixed convection flow of viscous, incompressible, electrically conducting fluid along a vertical stretching cylinder embedded in a porous medium in the presence of chemical reaction. The x-axis is taken along the stretching surface in the direction of the motion while the y-axis is perpendicular to the surface ,which is shown in Fig. 1. The continuity, momentum, energy and concentration equations governing such type of flow can be written as (Mukhopadhyay [29], Mukhopadhyay [30] and Mukhopadhyay [32]):.

$$\frac{\partial(ru)}{\partial x}+\frac{\partial(rv)}{\partial r}=0 \tag{1}$$

$$u\frac{\partial u}{\partial x}+v\frac{\partial u}{\partial y}=\frac{\upsilon}{r}\frac{\partial}{\partial r}\left(r\frac{\partial u}{\partial r}\right)-\frac{\sigma B_0^2}{\rho}u-\frac{\upsilon}{k'}u+g\beta(T-T_\infty)+g\beta^*(C-C_\infty) \tag{2}$$

$$u\frac{\partial T}{\partial x}+v\frac{\partial T}{\partial r}=\frac{\alpha}{r}\frac{\partial}{\partial r}\left(r\frac{\partial T}{\partial r}\right) \tag{3}$$

$$u\frac{\partial C}{\partial x}+v\frac{\partial C}{\partial r}=\frac{D}{r}\frac{\partial}{\partial r}\left(r\frac{\partial C}{\partial r}\right)-\Gamma(C-C_\infty) \tag{4}$$

where u and v are the velocity components in the x and r directions, respectively, υ is the kinematic viscosity, σ is the electrical conductivity, ρ is the density of the fluid, B_0 is the uniform magnetic field, υ is the kinematic viscosity, k' is the permeability of the medium, g is the gravity field, β is the coefficient of thermal expansion, β^* is the coefficient of expansion with concentration, T is the temperature, T_∞ is the temperature of the ambient fluid, C is the concentration, C_∞ is the concentration of the ambient fluid, α is the thermal diffusivity of the fluid, D is the mass diffusion coefficient, and Γ is the reaction rate constant of the solute.

The boundary conditions for the problem are:

$$u=U(x)+B_1\upsilon\frac{\partial u}{\partial r},\quad v=0,\quad T=T_w(x),\quad C=C_w(x)\quad \text{at}\quad r=R$$

$$u\to 0,\quad T\to T_\infty,\quad C\to C_\infty\quad \text{as}\quad r\to\infty \tag{5}$$

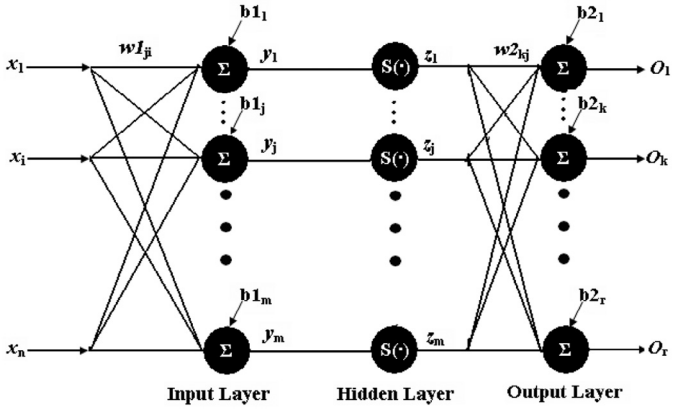

Fig. 2. Schematic diagram of BPNN.

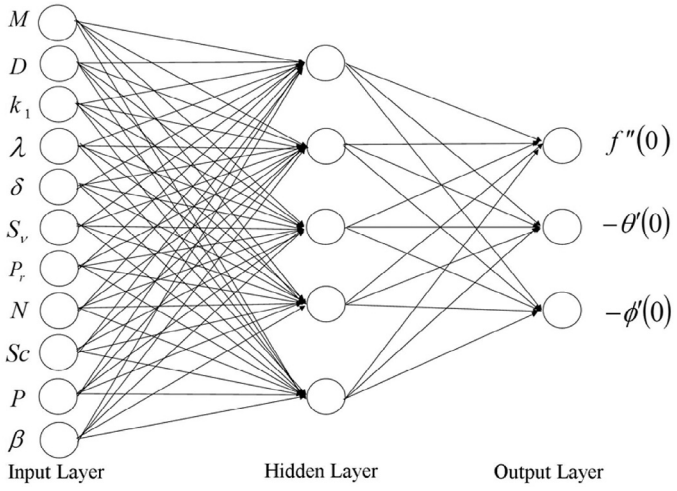

Fig. 3. Schematic diagram of a multi-layer ANN.

where $U(x)=U_0\left(\frac{x}{L}\right)$ is the stretching velocity, $T_w(x)=T_\infty+T_0\left(\frac{x}{L}\right)^N$ is the prescribed surface temperature, $C_w(x)=C_\infty+C_0\left(\frac{x}{L}\right)^P$ is the prescribed surface concentration, $U_0$is the reference velocity, T_0 is the reference temperature, C_0 is the reference concentration, L is the characteristic length, N is the temperature exponent, P is the concentration exponent, and B_1 is the velocity slip.

We introduce the similarity variables as

$$\eta=\frac{r^2-R^2}{2R}\sqrt{\left(\frac{U}{\upsilon x}\right)},\quad \psi=\sqrt{U\upsilon x}Rf(\eta),\quad \theta=\frac{T-T_\infty}{T_w-T_\infty},\quad \phi=\frac{C-C_\infty}{T_w-T_\infty} \tag{6}$$

where η is the similarity variable and $\psi(x,y)$ is the stream function. The velocity components are defined by $u=\frac{1}{r}\frac{\partial\psi}{\partial r}, v=-\frac{1}{r}\frac{\partial\psi}{\partial x}$.

Now substituting (6) into the Equations (2)–(4) and (5), we get the following set of ordinary differential equations:

$$(1+2M\eta)f'''+2Mf''+ff''-(f')^2-(\mathrm{D}+k_1)f'+\lambda\theta+\delta\phi=0 \tag{7}$$

$$(1+2M\eta)\theta''+2M\theta'+\Pr(f\theta'-Nf'\theta)=0 \tag{8}$$

$$(1+2M\eta)\phi''+2M\phi'+Sc(f\phi'-Pf'\phi-\beta\phi)=0 \tag{9}$$

with the boundary conditions

$$f=0,\quad f'=1+S_vf''(0),\quad \theta=1,\quad \phi=1\quad \text{at}\quad \eta=0$$

$$f'\to0,\quad \theta\to0,\quad \phi\to0\quad \text{as}\quad \eta\to\infty \tag{10}$$

where the prime denotes differentiation with respect to η, $M=\sqrt{\frac{\upsilon L}{U_0R^2}}$ is the curvature parameter, $D=\frac{\sigma B_0^2L}{\rho U_0}$ is the magnetic parameter, $k_1=\frac{\upsilon L}{k'U_0}$ is the permeability parameter, $\lambda=\frac{g\beta T_0L^2}{U_0^2}$ is the Grashof number, $\delta=\frac{g\beta^*C_0L^2}{U_0^2}$ is the solutal Grashof number, $\Pr=\frac{\upsilon}{\alpha}$ is the Prandtl number, $Sc=\frac{\nu}{D}$ is the Schmidt number, $\beta=\frac{\Gamma L}{U_0}$ is the chemical reaction parameter and $S_v=B_1\sqrt{\frac{\upsilon U_0}{L}}$ is the velocity slip. It should be noted that $M=0$ corresponds to the case of stretching flat plate and the no slip condition is recovered for $B_1=0$.

The quantities of physical interest in this problem are the skin-friction coefficient, heat transfer rate and mass transfer, and are defined as:

$$C_f=\frac{\tau_w}{\rho U^2/2},\quad Nu_x=\frac{xq_w}{k(T_w-T_\infty)}\quad\text{and}\quad Sh_x=\frac{xJ_w}{D(C_w-C_\infty)} \tag{11}$$

Respectively, the surface shear stress τ_w, surface heat flux q_w and mass flux J_w are given by:

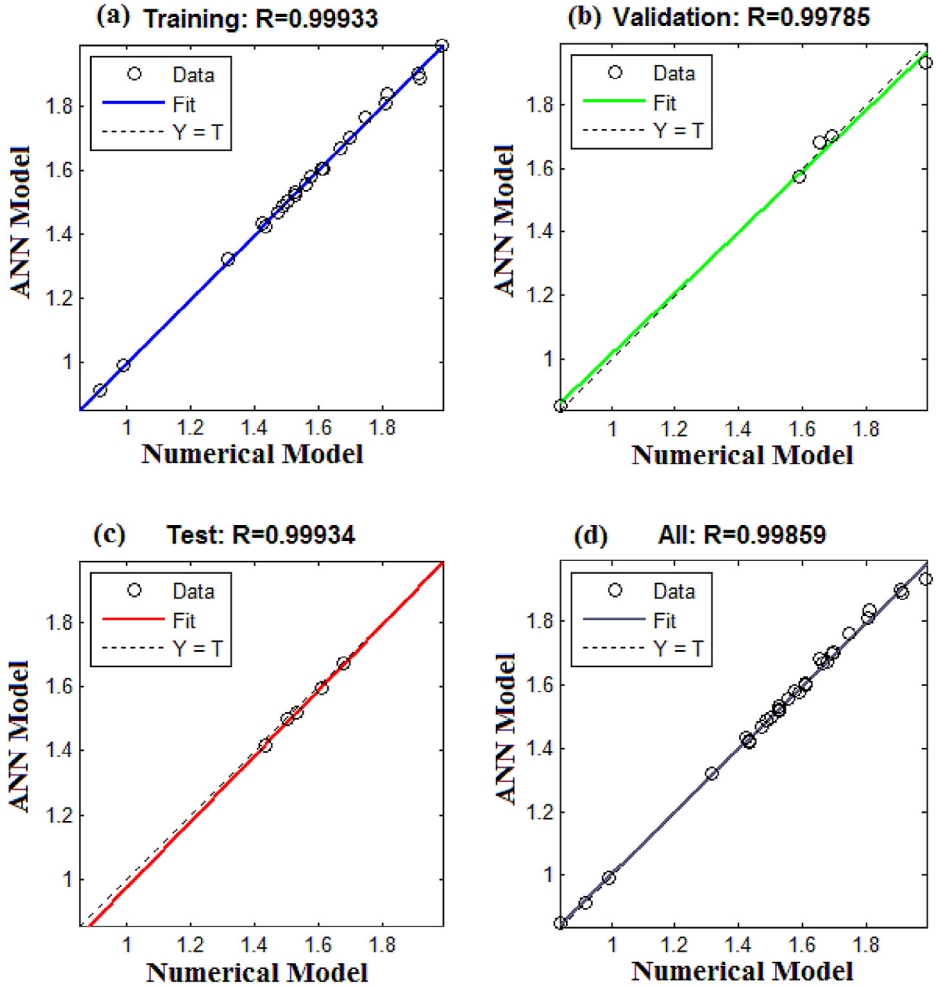

Fig. 4. Graphical representation of the skin friction coefficient.

$$\tau_w = \mu\left(\frac{\partial u}{\partial y}\right)_{y=0}, \quad q_w = -k\left(\frac{\partial T}{\partial y}\right)_{y=0} \quad \text{and} \quad J_w = -D\left(\frac{\partial C}{\partial y}\right)_{y=0} \tag{12}$$

Substituting (6) and (12) into Equation (11), we get:

$$\frac{1}{2}C_f\sqrt{\mathrm{Re}_x} = f''(0), \quad \frac{Nu_x}{\sqrt{\mathrm{Re}_x}} = -\theta'(0) \quad \text{and} \quad \frac{Sh_x}{\sqrt{\mathrm{Re}_x}} = -\phi'(0) \tag{13}$$

where $\mathrm{Re}_x = \frac{xU}{\upsilon}$ is the local Reynolds number.

3. Numerical modeling

Equations (7)–(9) along with the boundary conditions (10) form a two point boundary value problem. These equations are solved using shooting method, by converting them to an initial value problem. For this, we transform the non-linear ordinary differential Equations (7)–(9) to a system of first order differential equations as follows:

$$f' = z, \quad z' = p, \quad \mathrm{p}' = (z^2 - fp - 2Mp + (\mathrm{D} + k_1)z - \lambda\theta - \delta\phi) \tag{14}$$

$$\theta' = q, \quad q' = -[\mathrm{Pr}(fq - Nz\theta) + 2Mq]/(1 + 2M\eta) \tag{15}$$

$$\phi' = r, \quad r' = -[sc(fr - Pz\phi - \beta\phi) + 2Mr]/(1 + 2M\eta) \tag{16}$$

The boundary conditions (10) becomes:

$$f(0) = 0, \quad f'(0) = 1 + s_v\omega_1, \quad \omega_1 = f''(0), \quad \theta(0) = 1, \quad \phi(0) = 1 \tag{17}$$

In order to integrate (14)–(17) as an initial value problem, one requires a value for $p(0)$, i.e., $f''(0)$, $q(0)$, i.e., $\theta'(0)$ and $r(0)$, i.e., $\phi'(0)$, but no such values are given at the boundary. The suitable guess values for $\phi'(0)$ and $\phi'(0)$ are chosen and then integration is carried out. The most important factor of the shooting method is to choose an appropriate finite value of η_∞. In order to determine η_∞ for the boundary value problem, we start with some initial guess values for some particular set of physical parameters to obtain $f''(0), \theta'(0)$ and $\phi'(0)$. The solving procedure is repeated with another large value of η_∞ until two successive values of $f''(0), \theta'(0)$ and $\phi'(0)$ differ only by the specified significant digit. The last value of η_∞ is finally chosen to be the most appropriate value of the limit η_∞ for that particular set of parameters. The value of η_∞ may change for another set of physical parameters. Once the finite value of η_∞ is determined, then the integration is carried out. Compare the calculated values for f', θ and ϕ at $\eta = 10$(say) with the given boundary conditions $f'(10) = 0, \theta(10) = 0$, $\phi(10) = 0$ and adjust the estimated values, $f''(0), \theta'(0)$ and $\phi'(0)$ to give better approximation to the solution. We take the series values for $f''(0), \theta'(0)$, $\phi'(0)$ and apply the fourth order Runge–Kutta method with step size $h = 0.01$. The above procedure is repeated until the converged results up to the desired degree of accuracy 10^{-5} are achieved.

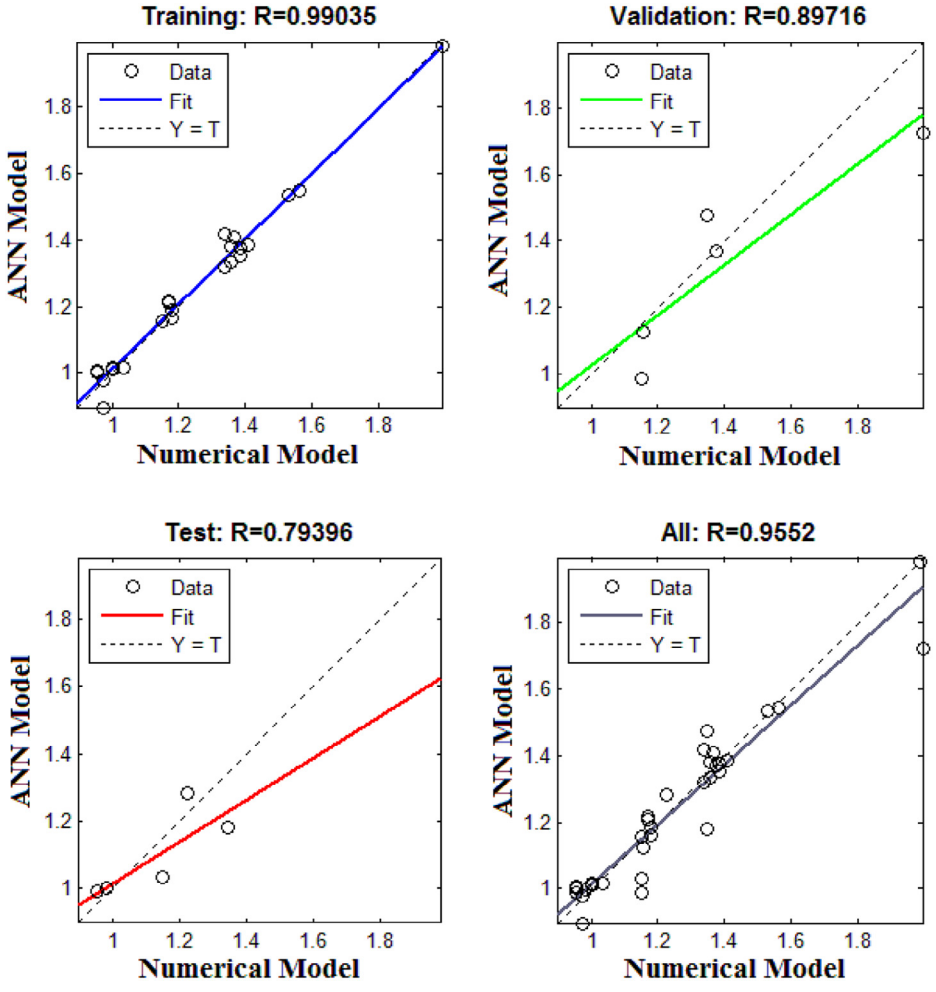

Fig. 5. Graphical representation of the Nusselt number.

4. Artificial neural network modeling

Artificial neural network (ANN) is a parallel processing architecture consisting of very simple and extremely interconnected processors called neurons organized in layers. Artificial neural network (ANN) is a mathematical model and advanced computing tool that processes information using neuro computing technique. ANN has the capability for machine learning and pattern matching. This model is developed from the human brain, having processing that is the same as that of the human biological neuron. The human brain is capable of doing vast calculations and utilizes billions of nerve cells existing in our brain. Biological neuron stores knowledge in memory bank, while in an ANN the data or the information is distributed through the network and stored in the form of weighted interconnection. The architecture of ANN model is shown in Fig. 2. This ANN model is different from conventional computation. ANN has been shown to be highly flexible modeling tool with the capability of learning the mathematical mapping between input and output. ANN is composed of layers of neurons. The input layer of neurons is connected to the output layers of neurons through one or more hidden layers of neurons. ANN is trained with experimental data and tested with other experimental data to reach at an optimum topology and weights. A multilayer perception (MLP) is feed forward neural network with one or more hidden layers.

Table 1
Comparison $f''(0)$ for several values of magnetic parameter in the absence of curvature parameter, porous medium, velocity slip, mixed convection parameter, concentration buoyancy parameter, temperature exponent, concentration exponent, Schmidt number and chemical reaction parameter.

D	Vajravelu et al. [33]	Numerical $f''(0)$	ANN $f''(0)$
0	1.000001	1.000001	1.000001
0.5	1.224745	1.224745	1.224745
1.0	1.414214	1.414213	1.414214
1.5	1.581139	1.581140	1.581139
2.0	1.732051	1.732050	1.732051

During the training process ANN adjusts its weights to minimize the errors between the predicted result and actual output by using Back Propagation algorithm.

A schematic diagram of a Back Propagation Neural Network (BPNN) with n inputs nodes, r outputs nodes and a single hidden layer of m nodes is shown in Fig. 2. Each interconnection between the nodes has a weight associate with it. The input nodes have a transfer function of unity and the activation function of the hidden and output nodes are sigmoidal $S(\bullet)$ and linear, respectively.

According to Fig. 2 the net input to the j^{th} hidden neuron is given by:

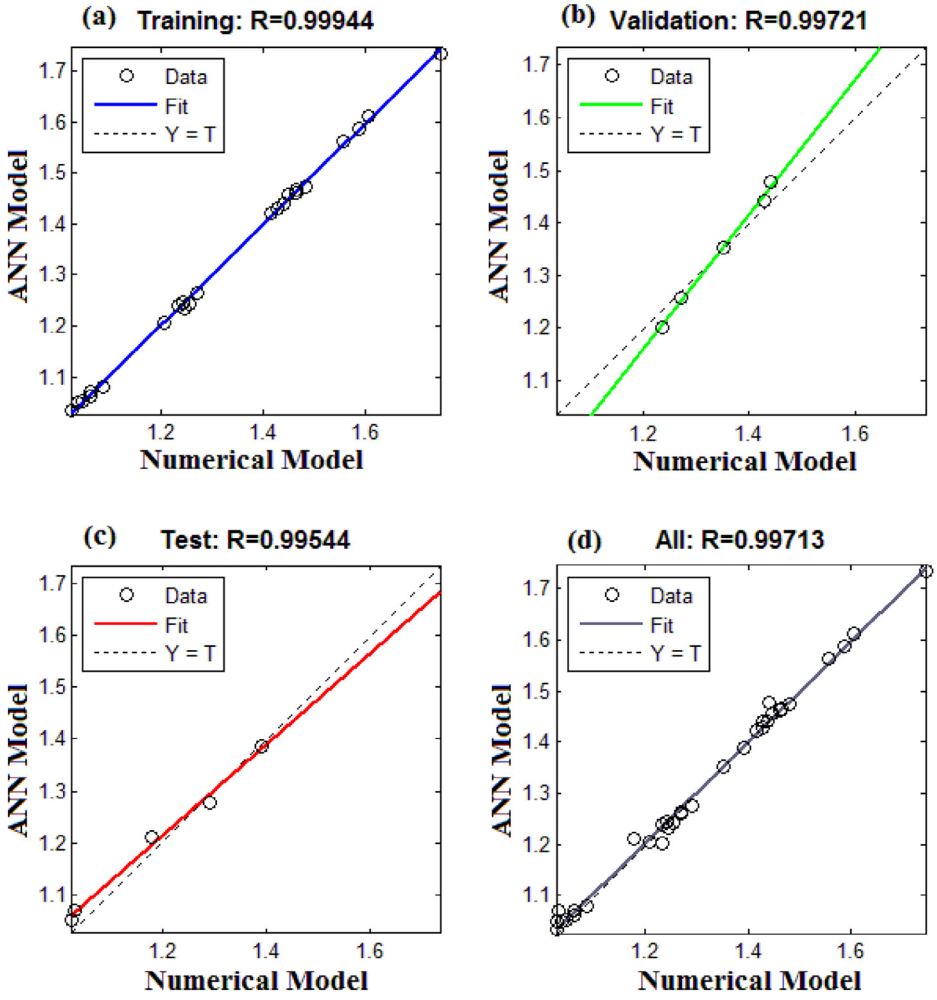

Fig. 6. Graphical representation of the Sherwood number.

$$y_j(x) = \sum_{i=1}^{n} w1_{ji} x_i + b1_j \tag{18}$$

where $w1_{ji}$ is the weight between the i^{th} node of input layer and j^{th} node of hidden layer and $b1_j$ is the bias at j^{th} node of hidden layer. The output of the j^{th} hidden node is defined by

$$z_j(x) = \frac{1}{1+e^{-y_j(x)}} \tag{19}$$

Given an input vector x, the output value $o_k(x)$ of the kth node of output layer is equal to the sum of the weighted outputs of the hidden nodes and the bias of the kth node output layer, and is given by:

$$o_k(x) = \sum_{j=1}^{m} w2_{kj} z_j + b2_k \tag{20}$$

where $w2_{kj}$ is the weight between the j^{th} node of hidden layer and kth node of output layer, $b2_k$ is biasing term at the k^{th} output node, and $b2_k$ is the biasing term at the kth node of output layer.

The output of ANN was determined by giving the inputs and computing the output from various nodes activation and interconnection weights. The output was compared to the experimental output and the mean squared error was calculated. The error value was then propagated backwards through the network and changes were made to the weights at each node in each layer. The whole process was repeated, in an iterative fashion, until the overall error value drops below a predetermined threshold.

In the present study, the numerical values obtained for all the parameters were used to train the ANN. The BPNN consists of three phases – namely the training, validation and test phases. The eleven parameters (M, D, k_1, λ, δ, S_v, Pr, N, Sc, P and β) determined for the samples used in the study were used as the input nodes, and three parameters (skin friction coefficient, Nusselt number and the Sherwood number) in these samples were used as the output parameter of the ANN, as shown in Fig. 3. As there exists no proper rule for setting the exact number of neurons in the hidden layer to avoid overfitting or underfitting of the input parameters and to make the learning phase convergent, the number of nodes in the hidden layer was selected through a trial and error method based

Table 2
Comparison $-\theta'(0)$ for several values of temperature exponent in the absence of curvature parameter, magnetic parameter, porous medium, velocity slip, mixed convection parameter, concentration buoyancy parameter, Schmidt number and chemical reaction parameter with Pr = 1.

N	Ishak and Nazar [26]	Grubka and Bobba [10]	Ali [2]	Mukhopadhyay [29]	Numerical $f''(0)$	ANN $f''(0)$
−2	−1.0000	–	–	–	−0.9999	−1.0000
−1	0.0000	–	–	–	0.0000	0.0000
0	0.5820	0.5820	0.5801	0.5821	0.5820	0.5820
1	1.0000	1.0000	0.9961	1.0000	1.0001	1.0001
2	1.3333	1.3333	1.3332	1.3332	1.3333	1.3333

Table 3
Values of $f''(0)$ for the various values of D, k_1, λ, δ, S_v, Pr, N, Sc, P and β.

M	D	k_1	λ	δ	S_v	Pr	N	Sc	P	β	Numerical $f''(0)$	ANN $f''(0)$
0.0	0.5	0.5	5.0	5.0	0.1	0.72	0.5	0.6	0.5	0.5	1.74792	1.763073917
0.0	1.0	0.5	5.0	5.0	0.1	0.72	0.5	0.6	0.5	0.5	1.52627	1.520320746
0.0	0.5	1.0	5.0	5.0	0.1	0.72	0.5	0.6	0.5	0.5	1.52627	1.532139794
0.0	0.5	0.5	6.0	5.0	0.1	0.72	0.5	0.6	0.5	0.5	1.98865	1.934049284
0.0	0.5	0.5	5.0	6.0	0.1	0.72	0.5	0.6	0.5	0.5	1.98637	1.99128844
0.0	0.5	0.5	5.0	5.0	0.5	0.72	0.5	0.6	0.5	0.5	0.99038	0.99155112
0.0	0.5	0.5	5.0	5.0	0.1	1.00	0.5	0.6	0.5	0.5	1.65453	1.682657116
0.0	0.5	0.5	5.0	5.0	0.1	0.72	1.0	0.6	0.5	0.5	1.67913	1.676297932
0.0	0.5	0.5	5.0	5.0	0.1	0.72	0.5	1.0	0.5	0.5	1.61098	1.604403182
0.0	0.5	0.5	5.0	5.0	0.1	0.72	0.5	0.6	1.0	0.5	1.69329	1.699698112
0.0	0.5	0.5	5.0	5.0	0.1	0.72	0.5	0.6	0.5	1.0	1.69738	1.702960861
0.5	0.5	0.5	5.0	5.0	0.1	0.72	0.5	0.6	0.5	0.5	1.66703	1.669329736
0.5	1.0	0.5	5.0	5.0	0.1	0.72	0.5	0.6	0.5	0.5	1.43185	1.418166739
0.5	0.5	1.0	5.0	5.0	0.1	0.72	0.5	0.6	0.5	0.5	1.43185	1.423882368
0.5	0.5	0.5	6.0	5.0	0.1	0.72	0.5	0.6	0.5	0.5	1.91479	1.888398577
0.5	0.5	0.5	5.0	6.0	0.1	0.72	0.5	0.6	0.5	0.5	1.91082	1.901597585
0.5	0.5	0.5	5.0	5.0	0.5	0.72	0.5	0.6	0.5	0.5	0.91857	0.914288975
0.5	0.5	0.5	5.0	5.0	0.1	1.00	0.5	0.6	0.5	0.5	1.57581	1.580271409
0.5	0.5	0.5	5.0	5.0	0.1	0.72	1.0	0.6	0.5	0.5	1.59299	1.57579867
0.5	0.5	0.5	5.0	5.0	0.1	0.72	0.5	1.0	0.5	0.5	1.52976	1.518738523
0.5	0.5	0.5	5.0	5.0	0.1	0.72	0.5	0.6	1.0	0.5	1.60985	1.598835568
0.5	0.5	0.5	5.0	5.0	0.1	0.72	0.5	0.6	0.5	1.0	1.61189	1.605602386
1.0	0.5	0.5	5.0	5.0	0.1	0.72	0.5	0.6	0.5	0.5	1.55893	1.554521832
1.0	1.0	0.5	5.0	5.0	0.1	0.72	0.5	0.6	0.5	0.5	1.31667	1.321386498
1.0	0.5	1.0	5.0	5.0	0.1	0.72	0.5	0.6	0.5	0.5	1.31667	1.320395723
1.0	0.5	0.5	6.0	5.0	0.1	0.72	0.5	0.6	0.5	0.5	1.81201	1.835549318
1.0	0.5	0.5	5.0	6.0	0.1	0.72	0.5	0.6	0.5	0.5	1.80735	1.810393176
1.0	0.5	0.5	5.0	5.0	0.5	0.72	0.5	0.6	0.5	0.5	0.83771	0.852424236
1.0	0.5	0.5	5.0	5.0	0.1	1.00	0.5	0.6	0.5	0.5	1.47448	1.468063705
1.0	0.5	0.5	5.0	5.0	0.1	0.72	1.0	0.6	0.5	0.5	1.48659	1.486537583
1.0	0.5	0.5	5.0	5.0	0.1	0.72	0.5	1.0	0.5	0.5	1.42621	1.433204407
1.0	0.5	0.5	5.0	5.0	0.1	0.72	0.5	0.6	1.0	0.5	1.50307	1.50012747
1.0	0.5	0.5	5.0	5.0	0.1	0.72	0.5	0.6	0.5	1.0	1.50314	1.498128279
MSE = 0.000207												

Table 4
Values of $-\theta'(0)$ for the various values of D, k_1, λ, δ, S_v, Pr, N, Sc, P and β.

M	D	k_1	λ	δ	S_v	Pr	N	Sc	P	β	Numerical $-\theta'(0)$	ANN $-\theta'(0)$
0.0	0.5	0.5	5.0	5.0	0.1	0.72	0.5	0.6	0.5	0.5	0.98138	0.997266
0.0	1.0	0.5	5.0	5.0	0.1	0.72	0.5	0.6	0.5	0.5	0.95499	1.000858
0.0	0.5	1.0	5.0	5.0	0.1	0.72	0.5	0.6	0.5	0.5	0.95499	0.98949
0.0	0.5	0.5	6.0	5.0	0.1	0.72	0.5	0.6	0.5	0.5	1.00244	1.016739
0.0	0.5	0.5	5.0	6.0	0.1	0.72	0.5	0.6	0.5	0.5	1.00222	1.011748
0.0	0.5	0.5	5.0	5.0	0.5	0.72	0.5	0.6	0.5	0.5	1.03373	1.015892
0.0	0.5	0.5	5.0	5.0	0.1	1.00	0.5	0.6	0.5	0.5	1.15829	1.123949
0.0	0.5	0.5	5.0	5.0	0.1	0.72	1.0	0.6	0.5	0.5	1.17919	1.186686
0.0	0.5	0.5	5.0	5.0	0.1	0.72	0.5	1.0	0.5	0.5	0.95442	1.007852
0.0	0.5	0.5	5.0	5.0	0.1	0.72	0.5	0.6	1.0	0.5	0.97235	0.979221
0.0	0.5	0.5	5.0	5.0	0.1	0.72	0.5	0.6	0.5	1.0	0.97194	0.896833
0.5	0.5	0.5	5.0	5.0	0.1	0.72	0.5	0.6	0.5	0.5	1.17810	1.163209
0.5	1.0	0.5	5.0	5.0	0.1	0.72	0.5	0.6	0.5	0.5	1.15050	1.032169
0.5	0.5	1.0	5.0	5.0	0.1	0.72	0.5	0.6	0.5	0.5	1.15050	1.154456
0.5	0.5	0.5	6.0	5.0	0.1	0.72	0.5	0.6	0.5	0.5	1.99550	1.722184
0.5	0.5	0.5	5.0	6.0	0.1	0.72	0.5	0.6	0.5	0.5	1.98970	1.98235
0.5	0.5	0.5	5.0	5.0	0.5	0.72	0.5	0.6	0.5	0.5	1.22461	1.282245
0.5	0.5	0.5	5.0	5.0	0.1	1.00	0.5	0.6	0.5	0.5	1.35006	1.476187
0.5	0.5	0.5	5.0	5.0	0.1	0.72	1.0	0.6	0.5	0.5	1.37836	1.370359
0.5	0.5	0.5	5.0	5.0	0.1	0.72	0.5	1.0	0.5	0.5	1.15388	0.986369
0.5	0.5	0.5	5.0	5.0	0.1	0.72	0.5	0.6	1.0	0.5	1.16918	1.21675
0.5	0.5	0.5	5.0	5.0	0.1	0.72	0.5	0.6	0.5	1.0	1.16866	1.210029
1.0	0.5	0.5	5.0	5.0	0.1	0.72	0.5	0.6	0.5	0.5	1.36609	1.40971
1.0	1.0	0.5	5.0	5.0	0.1	0.72	0.5	0.6	0.5	0.5	1.33962	1.318797
1.0	0.5	1.0	5.0	5.0	0.1	0.72	0.5	0.6	0.5	0.5	1.33962	1.417767
1.0	0.5	0.5	6.0	5.0	0.1	0.72	0.5	0.6	0.5	0.5	1.38721	1.375243
1.0	0.5	0.5	5.0	6.0	0.1	0.72	0.5	0.6	0.5	0.5	1.38658	1.353162
1.0	0.5	0.5	5.0	5.0	0.5	0.72	0.5	0.6	0.5	0.5	1.40745	1.386226
1.0	0.5	0.5	5.0	5.0	0.1	1.00	0.5	0.6	0.5	0.5	1.53114	1.536548
1.0	0.5	0.5	5.0	5.0	0.1	0.72	1.0	0.6	0.5	0.5	1.56285	1.54623
1.0	0.5	0.5	5.0	5.0	0.1	0.72	0.5	1.0	0.5	0.5	1.34573	1.179531
1.0	0.5	0.5	5.0	5.0	0.1	0.72	0.5	0.6	1.0	0.5	1.35829	1.333864
1.0	0.5	0.5	5.0	5.0	0.1	0.72	0.5	0.6	0.5	1.0	1.35774	1.37973
MSE = 0.005861												

on the number of epochs needed to train the network. After such iterative procedures it was found that the convergence between the numerical values and predicted values of skin friction, Nusselt number and Sherwood number was achieved with the inclusion of one hidden layer with five neurons. ANN structure has been designed and accomplished using the MATLAB code. A sigmoid function has been used as the activation function of artificial neurons, and training has been completed using a fixed (105) number of epochs. The total 33 numerical results were used to train, validate and test the ANN model for the skin friction coefficient. The 23 data sets were used for the training set, 5 data sets were used for validation, and the rest of the data were used for testing the results of the model. The performances of the skin friction coefficient, Nusselt number and Sherwood number for training, validation and test sets of the proposed ANN model are shown in Figs. 4, 5 and 6, respectively. From Tables 3, 4 and 5, the MSE values of the model for all data set were 0.000207, 0.005861 and 0.00022, respectively. It is observed that the ANN models were properly trained, as they simulate complicated relationship between the input and output variables. Moreover, the predicted skin friction coefficient, Nusselt number and Sherwood number values from the ANN model for training, validation and test sets are compared with numerically obtained skin friction coefficient, Nusselt number and Sherwood number values, which are given in Figs. 4, 5 and 6, respectively. The results obtained from the ANN model are in very good agreement with the numerical results. This study so far reveals that skin friction, Nusselt number and Sherwood number can alternatively be modeled using the ANN within a reasonable accuracy. The results obtained from the ANN model are in very good agreement with the numerical results.

To assess the validity and accuracy of the applied numerical scheme, the numerical values for the skin friction coefficient and heat transfer coefficient are compared with the available results, and the outcome is shown in Tables 1 and 2. It is observed that the present results are found to be in excellent agreement. The values of skin friction coefficient, Nusselt number and the Sherwood number for various values of the involved pertinent parameters are shown in Tables 3, 4 and 5. It can be noted that the skin friction coefficient decreases with increasing values of magnetic parameter, permeability parameter, slip velocity, Prandtl number, temperature exponent, Schmidt number, concentration exponent and chemical reaction parameter, whereas the reverse trend is observed in the case of Grashof number and solutal Grashof number. It is analyzed that the Nusselt number decreases with an increase in the magnetic parameter, permeability parameter, Schmidt number, concentration exponent and chemical reaction parameter, whereas it increases with an increase in the Grashof number and solutal Grashof number, slip velocity, Prandtl number and temperature exponent. It is viewed that the Sherwood number decreases as the magnetic parameter, permeability parameter, Prandtl number and temperature exponent. It can be seen that the Sherwood number increases with increasing Grashof number, and solutal Grashof number, velocity slip, Schmidt number, concentration exponent and chemical reaction parameter are raised. The results obtained from the numerical modeling and ANN model are in very good agreement with the numerical results. Thus according to the findings of the current study, the proposed ANN model is altogether for MHD boundary layer slip flow over a stretching cylinder embedded in a porous medium with chemical reaction, successfully.

5. Conclusions

In this study we successfully employed the ANN approach for the prediction of the magnetohydrodynamic convective boundary

Table 5
Values of $-\phi'(0)$ for the various values of D, k_1, λ, δ, S_v, Pr, N, Sc, P and β.

M	D	k_1	λ	δ	S_v	Pr	N	Sc	P	β	Numerical $-\phi'(0)$	ANN $-\phi'(0)$
0.0	0.5	0.5	5.0	5.0	0.1	0.72	0.5	0.6	0.5	0.5	1.04611	1.052205
0.0	1.0	0.5	5.0	5.0	0.1	0.72	0.5	0.6	0.5	0.5	1.02664	1.034671
0.0	0.5	1.0	5.0	5.0	0.1	0.72	0.5	0.6	0.5	0.5	1.02664	1.050425
0.0	0.5	0.5	6.0	5.0	0.1	0.72	0.5	0.6	0.5	0.5	1.06205	1.06102
0.0	0.5	0.5	5.0	6.0	0.1	0.72	0.5	0.6	0.5	0.5	1.06188	1.070736
0.0	0.5	0.5	5.0	5.0	0.5	0.72	0.5	0.6	0.5	0.5	1.08757	1.081142
0.0	0.5	0.5	5.0	5.0	0.1	1.00	0.5	0.6	0.5	0.5	1.03233	1.069896
0.0	0.5	0.5	5.0	5.0	0.1	0.72	1.0	0.6	0.5	0.5	1.03779	1.050276
0.0	0.5	0.5	5.0	5.0	0.1	0.72	0.5	1.0	0.5	0.5	1.35153	1.351746
0.0	0.5	0.5	5.0	5.0	0.1	0.72	0.5	0.6	1.0	0.5	1.20749	1.206541
0.0	0.5	0.5	5.0	5.0	0.1	0.72	0.5	0.6	0.5	1.0	1.17818	1.210674
0.5	0.5	0.5	5.0	5.0	0.1	0.72	0.5	0.6	0.5	0.5	1.25447	1.241803
0.5	1.0	0.5	5.0	5.0	0.1	0.72	0.5	0.6	0.5	0.5	1.23419	1.201676
0.5	0.5	1.0	5.0	5.0	0.1	0.72	0.5	0.6	0.5	0.5	1.23419	1.239793
0.5	0.5	0.5	6.0	5.0	0.1	0.72	0.5	0.6	0.5	0.5	1.27062	1.263844
0.5	0.5	0.5	5.0	6.0	0.1	0.72	0.5	0.6	0.5	0.5	1.27020	1.258929
0.5	0.5	0.5	5.0	5.0	0.5	0.72	0.5	0.6	0.5	0.5	1.29142	1.276459
0.5	0.5	0.5	5.0	5.0	0.1	1.00	0.5	0.6	0.5	0.5	1.24244	1.245221
0.5	0.5	0.5	5.0	5.0	0.1	0.72	1.0	0.6	0.5	0.5	1.24595	1.232724
0.5	0.5	0.5	5.0	5.0	0.1	0.72	0.5	1.0	0.5	0.5	1.55659	1.561755
0.5	0.5	0.5	5.0	5.0	0.1	0.72	0.5	0.6	1.0	0.5	1.41597	1.421957
0.5	0.5	0.5	5.0	5.0	0.1	0.72	0.5	0.6	0.5	1.0	1.39134	1.387681
1.0	0.5	0.5	5.0	5.0	0.1	0.72	0.5	0.6	0.5	0.5	1.44781	1.456286
1.0	1.0	0.5	5.0	5.0	0.1	0.72	0.5	0.6	0.5	0.5	1.42806	1.428552
1.0	0.5	1.0	5.0	5.0	0.1	0.72	0.5	0.6	0.5	0.5	1.42806	1.441933
1.0	0.5	0.5	6.0	5.0	0.1	0.72	0.5	0.6	0.5	0.5	1.46384	1.465789
1.0	0.5	0.5	5.0	6.0	0.1	0.72	0.5	0.6	0.5	0.5	1.46337	1.462009
1.0	0.5	0.5	5.0	5.0	0.5	0.72	0.5	0.6	0.5	0.5	1.48074	1.474493
1.0	0.5	0.5	5.0	5.0	0.1	1.00	0.5	0.6	0.5	0.5	1.43802	1.440757
1.0	0.5	0.5	5.0	5.0	0.1	0.72	1.0	0.6	0.5	0.5	1.44024	1.478707
1.0	0.5	0.5	5.0	5.0	0.1	0.72	0.5	1.0	0.5	0.5	1.74451	1.733712
1.0	0.5	0.5	5.0	5.0	0.1	0.72	0.5	0.6	1.0	0.5	1.60602	1.612186
1.0	0.5	0.5	5.0	5.0	0.1	0.72	0.5	0.6	0.5	1.0	1.58661	1.587253
MSE = 0.00022												

layer flow over a permeable stretching cylinder in the presence of chemical reaction. The developed ANN model is found to be reliable due to an excellent accuracy during the training, and validation and testing were compared with the numerical methods. The proposed ANN model is efficient, exact and time saving because it involves much less effort and yields results much faster than the numerical methods. Also, it is concluded that the designed ANN model may be considered as an alternative and powerful technique for solving the heat and mass transfer aspects with Newtonian/non-Newtonian fluid flow problems.

References

[1] L.J. Crane, Flow past a stretching plate, Z. Angew Math. Phys. 21 (1970) 645–647.
[2] M.E. Ali, Heat transfer characteristics of a continuous stretching surface, Heat Mass Transf. 29 (1994) 227–234.
[3] N. Bachok, A. Ishak, I. Pop, Unsteady boundary layer flow and heat transfer of a nano fluid over a permeable stretching/shrinking sheet, Int. J. Heat Mass Transf. 55 (2012) 2102–2109.
[4] K. Bhattacharyya, S. Mukhopadhyay, G.C. Layek, I. Pop, Effect of thermal radiation on micropolar fluid flow and heat transfer a porous shrinking sheet, Int. J. Heat Mass Transf. 55 (2012) 2945–2952.
[5] A.J. Chamka, Transient hydromagnetic three-dimensional natural convection from an inclined stretching permeable surface, Chem. Eng. J. 76 (2000) 159–168.
[6] A.S. Chethan, G.N. Sekhar, P.G. Siddheshwar, Flow and heat transfer of an exponential stretching sheet in viscoelastic liquid with Navier slip boundary condition, J. Appl. Fluid Mech. 8 (2) (2015) 223–229.
[7] R. Cortell, Viscous flow and heat transfer over a nonlinearly stretching sheet, Appl. Math. Comput. 184 (2) (2007) 864–873.
[8] K. Das, Effect of chemical reaction and thermal radiation on heat and mass transfer flow of MHD micropolar in a rotating frame of reference, Int. J. Heat Mass Transf. 54 (2011) 3505–3513.
[9] M. Farahi Sahari, A. Hossein Nezhad, Estimation of the flow and heat transfer in MHD flow of a power law fluid over a porous plate using artificial neural networks, Middle East J. Sci. Res. 22 (9) (2014) 1422–1429.
[10] L.J. Grubka, K.M. Bobba, Heat transfer characteristics of a continuous, stretching surface with variable temperature, ASME J, Heat Transf. 107 (1985) 248–250.
[11] T. Hayat, Z. Abbas, N. Ali, MHD flow and mass transfer of a upper–convected Maxwell fluid past a porous shrinking sheet with chemical reaction species, Phys. Lett. A 372 (2008) 4698–4704.
[12] T. Hayat, M. Hussain, A. Alsaedi, S.A. Shehzad, G.Q. Chen, Flow of power-law nanofluid over a stretching surface with Newtonian heating, J. Appl. Fluid Mech. 8 (2) (2015) 273–280.
[13] W. Ibrahim, B. Shanker, Unsteady MHD boundary-layer flow and heat transfer due to stretching sheet in the presence of heat source or sink, Comput. Fluids 70 (2012) 21–28.
[14] D. Pal, S. Chatterjee, Effects of radiation on Darcy-Forchheimer convective flow over a stretching sheet in a micropolar fluid with non-uniform heat source/sink, J. Appl. Fluid Mech. 8 (2) (2015) 207–212.
[15] S. Srinivas, P.B.A. Reddy, B.S.R.A. Prasad, Effects of chemical reaction and thermal radiation on MHD flow over an inclined permeable stretching surface with non-uniform heat source/sink: an application to the dynamics of blood flow, J. Mech. Med. Biol. 14 (2014) 1–24.
[16] S. Srinivas, P.B.A. Reddy, B.S.R.A. Prasad, Non-Darcian unsteady flow of a micropolar fluid over a porous stretching sheet with thermal radiation and chemical reaction, Heat Transf. Asian Res. 44 (2) (2015) 172–187.
[17] P.S. Gupta, A.S. Gupta, Heat and mass transfer on a stretching sheet with suction or blowing, Can. J. Chem. Eng. 55 (1977) 744–746.
[18] P.G. Siddheshwar, U.S. Mahabaleshwar, Effects of radiation and heat source on MHD flow of a viscoelastic liquid and heat transfer stretching sheet, Int. J. Nonlinear Mech. 40 (2005) 807–820.
[19] G. Colonna, M. Capitelli, Electron and vibrational kinetics in the boundary layer of hypersonic flow, J. Thermophys. Heat Transf. 10 (1996) 406–412.
[20] I. Armenise, M. Capitelli, G. Colonna, N. Koudriavtsev, V. Smetanin, Nonequilibrium vibrational kinetics during hypersonic flow of a solid body in nitrogen and its influence on the surface heat flux, Plasma Chem. Plasma Proc. 15 (3) (1995) 501–528.
[21] H.T. Lin, Y.P. Shih, Laminar boundary layer heat transfer along static and moving cylinders, J. Chin. Inst. Eng. 3 (1980) 73–79.
[22] H.T. Lin, Y.P. Shih, Buoyancy effects on the laminar boundary layer heat transfer along vertically moving cylinders, J. Chin. Inst. Eng. 4 (1981) 47–51.
[23] C.Y. Wang, Fluid flow due to a stretching cylinder, Phys. Fluids 31 (1998) 466–468.
[24] A.J. Chamka, M.M.A. Quadri, Heat and mass transfer from a permeable cylinder in a porous medium with magnetic field and heat generation/absorption effects, Numer. Heat Transf. A 40 (2001) 387–401.

[25] A. Ishak, R. Nazar, I. Pop, Magnetohydrodynamic (MHD) flow and heat transfer due to a stretching cylinder, Energy Convers. Manag. 49 (2008) 3265–3269.
[26] A. Ishak, R. Nazar, Laminar boundary layer flow along a stretching cylinder, Eur. J. Sci. Res. 36 (1) (2009) 22–29.
[27] N. Bachok, A. Ishak, Flow and heat transfer over a stretching cylinder with prescribed surface heat flux, Malaysian J. Math. Sci. 4 (2010) 159–169.
[28] W.K. Hussam, M.C. Thompson, G.J. Sheard, Dynamics and heat transfer in a Quasi two dimensional MHD flow past a circular cylinder in a duct at high Hartmann number, Int. J. Heat Mass Transf. 54 (2011) 1091–1100.
[29] S. Mukhopadhyay, Mixed convection boundary layer flow along a stretching cylinder in porous medium, J. Petrol. Sci. Eng. 96–97 (2012) 73–78.
[30] S. Mukhopadhyay, MHD boundary layer slip flow along a stretching cylinder, Ain Shams Eng. J. 4 (2013) 317–324.
[31] K. Vajravelu, K.V. Prasad, S.R. Santhi, V. Umesh, Fluid flow and heat transfer over a permeable stretching cylinder, J. Appl. Fluid Mech. 7 (1) (2014) 111–120.
[32] S. Mukhopadhyay, Chemically reactive solute transfer in a boundary layer slip flow along a stretching cylinder, Font Chem. Sci. Eng. 5 (3) (2011) 385–391.
[33] K. Vajravelu, K.V. Prasad, S.R. Santhi, Axisymmetric magnetohydrodynamic flow and heat transfer at a non-isothermal stretching cylinder, Appl. Math. Comput. 219 (2012) 3393–4005.